New Results for the Pointing Errors Model in Two Asymptotic Cases

Maoke Miao, Xiao-yu Chen, Rui Yin, and Jiantao Yuan

***Abstract*—Several precise and computationally efficient results for pointing errors models in two asymptotic cases are derived in this paper. The normalized mean-squared error (NMSE) performance metric is employed to quantify the accuracy of different models. For the case that the beam width is relatively larger than the detection aperture, we propose the three kinds of models that have the form of $c_1 \exp(-c_2 r^2)$. It is shown that the modified intensity uniform model not only achieves a comparable accuracy with the best linearized model, but also is expressed in an elegant mathematical way when compared to the traditional Farid model. This indicates that the modified intensity uniform model is preferable in the performance analysis of free space optical (FSO) systems considering the effects of the pointing errors. By analogizing the beam spot with a point in the case that beam width is smaller than the detection aperture, the solution of the pointing errors model is transformed to a smooth function approximation problem, and we find that a more accurate approximation can be achieved by the proposed point approximation model when compared to the model that is induced from the Vasylyev model in some scenarios.**

***Index Terms*—Pointing errors models, NMSE performance, farid model, FSO systems, Vasylyev model.**

I. Introduction

FREE-SPACE optical (FSO) is a wireless optical communication technology, which has attracted considerable attention in both academic and industry due to its great potential: larger bandwidth and high data rate, unregulated spectrum, low mass and less power requirements, rapid and easy deployment [1]. Also, FSO technology can be deployed together in the so-called hybrid radio frequency (RF)/FSO systems that are considered to be a promising solution for reliable wireless backhaul connectivity to enable long-range communications in future 6G networks [2]. Furthermore, the advanced reconfigurable intelligent surfaces (RIS) technology that was proposed recently, can be used to enhance the performance of FSO systems, and thus broadening the range of FSO communication [3].

Manuscript received 10 January 2023; revised 2 May 2023; accepted 9 May 2023. Date of publication 12 May 2023; date of current version 19 May 2023. This work was supported in part by the National Natural Science Foundation of China under Grant 61871347 and in part by the Scientific Research Foundation of Zhejiang University City College under Grant J-202321. *(Corresponding author: Maoke Miao.)*

Maoke Miao is with the School of Information Science and Electronic Engineering, Zhejiang University, Zhejiang 310027, China, and also with the School of Information and Electrical Engineering, Hangzhou City University, Hangzhou 310015, China (e-mail: maokemiao@zju.edu.cn).

Xiao-yu Chen, Rui Yin, and Jiantao Yuan are with the School of Information and Electrical Engineering, Hangzhou City University, Hangzhou 310015, China (e-mail: chenxiaoyu@zucc.edu.cn; yinrui@zucc.edu.cn; yuanjt@zucc.edu.cn).

Digital Object Identifier 10.1109/JPHOT.2023.3275578

Despite these benefits of FSO technology, the performance of FSO communication systems can be deteriorated by adverse effects, such as beam wandering and spreading, and scatting when the optical carrier propagates through atmospheric turbulence. It has been shown in [4] that turbulence-induced irradiance scintillation and pointing errors are the two major performance-limiting factors for FSO links with ranges longer than one kilometer. Note that the beam wander and mechanical vibration result in the pointing errors, and they have the same mathematical model with only differing in physical meaning of parameters [5], [6]. The research on the irradiance scintillation models have been studied extensively, and plenty of precise or mathematically tractable models have been proposed so far, such as Gamma-Gamma distribution [7], Fischer-Snedecor $\mathcal{F}$ distribution [8], lognormal-Rician distribution [9], and Málaga distribution [10]. Unfortunately, the results for the pointing errors models are greatly limited. To the best of the author's knowledge, the pointing errors model for a Gaussian beam was firstly developed by R. Esposito in [11], where it was expressed in terms of Marcum's Q function.[1] Subsequently, a simple and efficient approximation of this model was present by Farid [13], namely, Farid model, which has been widely used in FSO systems. It should be noted, however, the Farid model has two main drawbacks: 1) one is the low approximation accuracy when the radius of beam width is two times less than that of the detection aperture. 2) the other is that it requires the computation of the complex error function $\mathrm{erf}(\cdot)$. Recently, the other pointing errors model was established by Vasylyev in the field of quantum communication [14]. Although it provides a good approximation regardless of the relationship between beam width and detection aperture, its complicated mathematical form greatly hampers the analytic expression for the system performance.

In this work, we present some new results on the pointing errors model. Several computation-efficient models are proposed, and the accuracy of them is investigated in detail. For the case that the beam width is relatively larger than the detection aperture, the normalized mean-squared error (NMSE) performance indicates that the proposed modified intensity uniform model not only shows a better approximation accuracy than the Farid model, but also has a simpler expression. This is one of the key contributions of this paper. By analogizing the beam spot with a point in the case that beam width is smaller than the

[1]Marcum's Q function plays an important role in the performance analysis of communication systems, which is defined as $Q(\alpha,\beta) = \int_{\beta}^{\infty} t \exp(-(t^2+x^2)/2) I_0(\alpha t) dt$ [12].

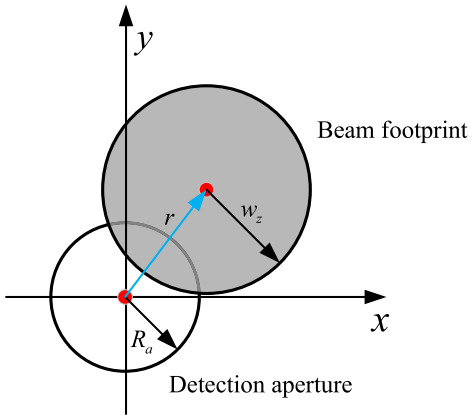

Fig. 1. Schematic description of the deflection distance r between the beam center and the detector center.

detection aperture, the solution of the pointing errors model is transformed to a smooth function approximation problem. Numerical results demonstrate that the proposed point approximation model provides a higher accuracy than the model induced from the Vasylyev model in some scenarios.

II. Pointing Errors Model

In line-of-sight FSO communication links, misalignment between transmitter and receiver results in pointing errors, which are the another performance-limiting factor besides turbulence-induced scintillation. We note that the pointing errors consist of two parts in practical FSO systems. One is the beam wandering caused by large scale eddy and the other is due to mechanical vibration or thermal expansion. However, the former can be dealt with in a similar methodology to the latter, as shown in [5], [6].

After propagating a distance z from the transmitter, the normalized spatial distribution of a Gaussian beam at the receiver plane is given by

$$I_{\text{beam}}(\boldsymbol{\rho}; z) = \frac{2}{\pi w_z^2} \exp\left(-\frac{2\|\boldsymbol{\rho}\|^2}{w_z^2}\right), \tag{1}$$

where $\boldsymbol{\rho}$ denotes the displacement from the beam center. According to [15], the beam radius w_z at the distance z is related to the beam waist w_0 at $z = 0$, wavelength λ, and atmospheric coherence length ρ_0, which can be expressed as

$$w_z \approx w_o \left[1 + \varepsilon \left(\frac{\lambda z}{\pi w_o^2}\right)^2\right]^{\frac{1}{2}}, \tag{2}$$

where $\varepsilon = (1 + 2w_o^2/\rho_o^2(z))$. Specifically, $\rho_0 = (0.55 C_n^2 k^2 z)^{-3/5}$ for the spherical wave with C_n^2 and $k = 2\pi/\lambda$ denoting the index of refraction structure constant and wave number respectively.

At the receiver, the effect of pointing errors causes the deflection between the beam center and aperture center, as shown in Fig. 1. Hence, the transmission efficiency within a circular detection aperture of radius R_a reads as

$$h_p(\boldsymbol{r}; z) = \int_{\mathcal{A}} I_{\text{beam}}(\boldsymbol{\rho} - \boldsymbol{r}; z) d\boldsymbol{\rho}, \tag{3}$$

where $\mathcal{A}$ is the detector area. Considering the symmetry of the beam shape and the detector area, $h_p(\boldsymbol{r}; z)$ depends on the radial distance $r = ||\boldsymbol{r}||$, which is given by

$$h_p(r; z) = \int_{-R_a}^{R_a} \int_{-\zeta}^{\zeta} \frac{2}{\pi w_z^2} \exp\left(-2\frac{(x-r)^2 + y^2}{w_z^2}\right) dy dx, \tag{4}$$

where $\zeta = \sqrt{R_a^2 - x^2}$. Equivalently, (4) can be expressed in terms of the incomplete Weber Integral, which is found to be [14], [16]

$$h_p(r; z) = \frac{4}{w_z^2} \exp\left(-2\frac{r^2}{w_z^2}\right) \int_0^{R_a} \varrho \exp\left(-2\frac{\rho^2}{w_z^2}\right) \times I_0\left(\frac{4}{w_z^2} r\varrho\right) \mathrm{d}\varrho, \tag{5}$$

where $I_n(\cdot)$ is the modified Bessel function. From (5), the pointing errors model at $r = 0$ can be easily derived as

$$h_p(r = 0; z) = 1 - \exp\left(-2\frac{R_a^2}{w_z^2}\right). \tag{6}$$

III. New Results of Pointing Errors Model in Two Asymptotic Cases

In this section, we provide several methods to evaluate the pointing errors model in two asymptotic cases: $w_z \gg R_a$ and $R_a \gg w_z$. In most current practical FSO systems, the divergence of emitted laser beam is typical of tens of μrad while the size of the receiving aperture is on the order of tens of centimeters [17], [18]. Hence, these two scenarios can occur, depending on the transmitted distance z.

A. Models for $w_z \gg R_a$.

We demonstrate that the expression for pointing errors has the form $h_p(r; z) = c_1 \exp(-c_2 r^2)$ by combing the condition $w_z \gg R_a$ and (1). Note that this simple form has the benefit to facilitate the performance analysis of FSO systems provided that the radial displacement r follows a Rayleigh distribution, which is given by

$$f_r(r) = \frac{r}{\sigma_s^2} \exp\left(-\frac{r^2}{2\sigma_s^2}\right), \quad r > 0 \tag{7}$$

where σ_s^2 is the jitter variance at the receiver. With (7), the unified probability density function (PDF) of h_p is obtained as

$$f_{h_p}(h_p) = \frac{\gamma^2}{c_1^{\gamma^2}} h^{\gamma^2 - 1}, \tag{8}$$

where $\gamma^2 = 1/(2\sigma_s^2 c_2)$. In what follows, we aim at determining the values of coefficients c_1 and c_2 for different pointing errors models. It should be emphasized that the present results in the following are expressed in terms of elementary functions, avoiding the computation of complicated function, that is, erfc$(\cdot)$ and $I_n(\cdot)$ in Farid model [13, eqn. (9)] and Vasylyev model [14, eqn. (D3)] respectively.

1) Intensity Uniform Model: It can be reasonably claimed that the intensity distribution within the area of detector aperture is approximately uniform when $w_z \gg R_a$, and we can regard the

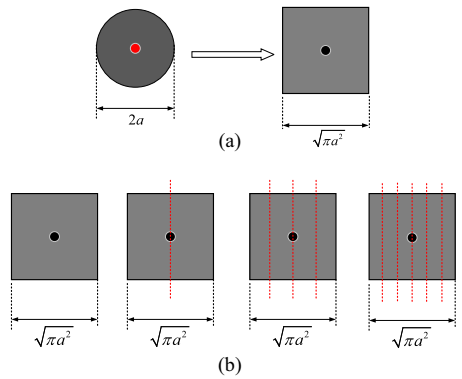

Fig. 2. Two parts of Linearized Model. (a) Transformation of equal area between the circle and the square. (b) Partition: Examples of 0, 2, 4, 6 partitions are shown from left to right respectively.

intensity of detector center as an intensity value of this area. As such, we have

$$h_p\left(r;z\right)=\pi R_a^2 I_{\text{beam}}\left(\boldsymbol{r};z\right)=\frac{2R_a^2}{w_z^2}\exp\left(-\frac{2r^2}{w_z^2}\right). \tag{9}$$

In this case, $c_1=2R_a^2/w_z^2$ and $c_2=2/w_z^2$.

2) Modified Intensity Uniform Model: Although the expression for the intensity uniform model is simple, it leaves out some important details. For example, $c_1=h_p(r=0;z)=\eta=1-\exp(-2R_a^2/w_z^2)$ according to (5) while it is $2R_a^2/w_z^2$ in intensity uniform model. Note that $2R_a^2/w_z^2$ is a Taylor series approximation of $1-\exp(-2R_a^2/w_z^2)$. Inspired by this result, coefficient c_2 in (9) may exhibit the same behaviour as the coefficient c_1, that is, $2/w_z^2$ is a Taylor approximation of some function. Specifically, we have

$$h_p\left(r;z\right)=\eta\exp\left(-\eta\frac{r^2}{R_a^2}\right). \tag{10}$$

when an exponential function is considered. From (10), we have $c_1=\eta$ and $c_2=\eta/R_a^2$.

3) Linearized Model: The coefficient c_1 in linearized model is $1-\exp(-2R_a^2/w_z^2)$, which is the same as that in modified intensity uniform model, and the coefficient c_2 is determined in another way. Fig. 2 depicts the process of solving the coefficient c_2, which consists of two steps: the circle-square transformation, and the equal space partition.[2]

To calculate the c_2 in this model, we assume that the equal space partition step only operates along one axis, and the intensity in each interval forms a linear relationship with the values from this axis while keeping the intensity same in the other axis. Specifically, the obtained result is independent of the axis due to the symmetry, and an example of the equal space partition along the x-axis is shown in Fig. 3, where $x_n-x_0=n\delta=\sqrt{\pi a^2}$ with n and δ denoting the number of splits and spacing respectively.

[2]The reason why we only carry out circular-square transformation and equal space segmentation are as follows: 1) (4) is difficult to solve analytically since the upper and lower limits of integration for the x- and y-axes satisfy the equation of a circle. However, the idea of "circular-square transformation" can be used to remove this relationship between them. 2) The "equal space segmentation" is inspired by the specific "uniform partition" in definite integral, which is the simplest method of partitioning.

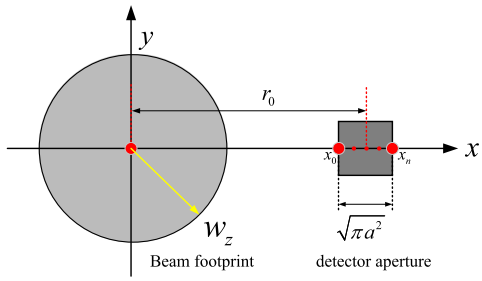

Fig. 3. Equal space partition along the x-axis.

Algorithm 1: Algorithm for the Determination of c_2 in *Linearized Model*.

Input: Radius of detector aperture R_a, beam radius w_z, number of splits n, radial distance r_0.
Output: The coefficient c_2.
Initialisation: $l=\sqrt{\pi R_a^2}$, $Q=0$, $c_1=1-\exp(-2R_a^2/w_z^2)$, $\delta=l/n$.
1: **for** $i=0$ to $n-1$ **do**
2: $k_i=(I_{\text{beam}}(r_0-l/2+\delta(i+1);z)-I_{\text{beam}}(r_0-l/2+\delta i;z))/\delta$.
3: $b_i=I_{\text{beam}}(r_0-l/2+\delta i;z)-k_i(r_0-l/2+\delta i)$.
4: $Q=Q+\sqrt{\pi R_a^2/4}\delta(k_i\delta+2x_i\delta+2b_i)$.
5: **end for**
$c_2=-\ln(Q/c_1)/r_0^2$.
6: **return** c_2

Hence, based on the above description, the intensity distribution satisfies the following relation

$$I_{\text{beam}}\left(x,y;z\right)\approx I_{\text{beam}}\left(x;z\right)=k_i x+b_i, x\in\left[x_i,x_{i+1}\right), \tag{11}$$

where $x_{i+1}=x_i+\delta$, k_i, b_i are the coefficients of a linear function in the i-th interval, and they can be determined by two distant points, i.e., $(x_i, I_{\text{beam}}(x_i;z))$ and $(x_{i+1}, I_{\text{beam}}(x_{i+1};z))$. Then, the pointing errors model $h_p(r;z)$ is approximated as

$$\begin{aligned}h_p\left(r;z\right)&\approx\sum_{i=0}^{n-1}\int_{-\sqrt{\pi R_a^2/4}}^{\sqrt{\pi R_a^2/4}}\int_{x_i}^{x_{i+1}}\left(k_i x+b_i\right)dxdy\\&\approx\sum_{i=0}^{n-1}\sqrt{\pi R_a^2/4}\delta\left(k_i\delta+2x_i\delta+2b_i\right).\end{aligned} \tag{12}$$

The detailed description of the procedure for the determination of c_2 in linearized model is provided below.[3]

4) Farid Model: According to [13], the Farid pointing errors model is expressed as

$$h_p(r;z)=A_0\exp\left(-\frac{2r^2}{w_{z_{\text{eq}}}^2}\right), \tag{13}$$

[3]Note that the radial distance r_0 can be optimized to improve the approximation accuracy of the linearized model. In the numerical section, we show that the normalized optimized parameter r_0^*/R_a has a quadratic relation with w_z/R_a, and this indicates that the number of inputs to this model can be reduced by one.

where $v = (\sqrt{\pi}a)/(\sqrt{2}w_z)$, and

$$A_0 = [\mathrm{erf}(v)]^2, \quad w_{z_{\mathrm{eq}}}^2 = w_z^2 \frac{\sqrt{\pi}\,\mathrm{erf}(v)}{2v\exp(-v^2)} \tag{14}$$

with A_0 and $w_{z_{eq}}$ denoting the fraction of the collected power at $r = 0$ and the equivalent beam width respectively.

According to (13), $c_1 = A_0$ and $c_2 = 2/w_{z_{eq}}^2$ for the Farid model.

5) First Reduced Vasylyev Model: According to [14], the pointing errors model established by Vasylyev is expressed as

$$h_p(r;z) = \eta \exp\left[-\left(\frac{r}{R}\right)^{\lambda}\right], \tag{15}$$

where λ and R are respectively given by

$$\begin{aligned}\lambda &= 8\frac{R_a^2}{w_z^2}\frac{\exp\left(-4\frac{R_a^2}{w_z^2}\right) I_1\left(4\frac{R_a^2}{w_z^2}\right)}{1-\exp\left(-4\frac{R_a^2}{w_z^2}\right) I_0\left(4\frac{R_a^2}{w_z^2}\right)} \\ &\quad \times \left[\ln\left(\frac{2\eta}{1-\exp\left[-4\frac{R_a^2}{w_z^2}\right] I_0\left(4\frac{R_a^2}{w_z^2}\right)}\right)\right]^{-1}, \\ R &= R_a\left[\ln\left(\frac{2\eta}{1-\exp\left(-4\frac{R_a^2}{w_z^2}\right) I_0\left(4\frac{R_a^2}{w_z^2}\right)}\right)\right]^{-\frac{1}{\lambda}}.\end{aligned} \tag{16}$$

By using the Taylor series of $\exp(\cdot)$, $I_0(\cdot)$, and $I_1(\cdot)$ at $R_a/w_z = 0$ in [19], coefficients λ and R are then simplified into

$$\begin{aligned}&\lim_{R_a/w_z\to 0} \lambda = 2 \\ &\lim_{R_a/w_z\to 0} R = R_a\left(2R_a^2/w_z^2\right)^{-1/2} = w_z/2\end{aligned} \tag{17}$$

after some algebraic manipulations. Substituting (17) into (15), the first reduced Vasylyev model is obtained as

$$h_p(r;z) = \eta \exp\left(-\frac{2r^2}{w_z^2}\right). \tag{18}$$

In this case, $c_1 = \eta$, $c_2 = 2/w_z^2$.

B. Models for $R_a \gg w_z$.

1) Point Approximation Model: In this model, beam spot acts like a *point*, as shown in Fig. 4. Note that nearly total energy of laser beam is concentrated around this point, and this leads to

$$h_p(r;z) = \begin{cases} 1 & 0 \le r < R_a \\ 0 & r > R_a \end{cases}. \tag{19}$$

Alternatively, the above formula can be rewritten as

$$h_p(r;z) = \varepsilon(r) - \varepsilon(r - R_a) \tag{20}$$

where $\varepsilon(\cdot)$ denotes the Heaviside step function. Specifically, the pointing errors at $r = R_a$ can be obtained as

$$h_p(r;z) = \int_0^{w_z} \frac{2}{\pi w_z^2}\exp\left(-\frac{2r^2}{w_z^2}\right) r\pi dr \approx \frac{1}{2}. \tag{21}$$

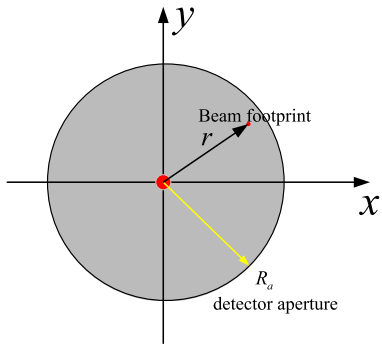

Fig. 4. Schematic description of point approximation of beam spot when $R_a \gg w_z$.

Combining (19) with (21), the pointing errors model for the case $R_a \gg w_z$ can then be expressed as

$$h_p(r;z) = \begin{cases} 1 & 0 \le r < R_a \\ 1/2 & r = R_a \\ 0 & r > R_a \end{cases}. \tag{22}$$

The problem is then transformed to find some smooth function that can approximates (22) efficiently. Inspired by the fact that the logistic function is typically used to approximate the step function, and we develop a pointing errors formula as [4]

$$h_p(r;z) \approx 1 - \frac{1}{1+\exp\left(-\alpha\left[\left(\frac{r}{R_a}\right)^{2k} - 1\right]\right)}, \tag{23}$$

where $k \in \mathbb{Z}^+$ with $\mathbb{Z}^+$ denoting the set of positive integers, and α represents the logistic growth rate or steepness of the curve.

From (23), the derivative of $h_p(r;z)$ at $r = R_a$ results to a simple formula, which is obtained as

$$\left.\frac{dh_p(r;z)}{dr}\right|_{r=R_a} = -\frac{k}{2}\alpha. \tag{24}$$

Hence, combining (24) with [14, eqn. (D6)], the relationship between k and α is given by

$$\alpha = \frac{8R_a^2}{kw_z^2}\exp\left(-4\frac{R_a^2}{w_z^2}\right) I_1\left(4\frac{R_a^2}{w_z^2}\right). \tag{25}$$

In addition, by using the asymptotic expansion formula of the modified Bessel function $I_n(z)$ for large z in [21], i.e., $I_n(nz) \approx (2\pi nz)^{-\frac{1}{2}}\exp(nz)$, and then (25) reduces into

$$\alpha = \frac{2\sqrt{2}R_a}{\sqrt{\pi}kw_z}. \tag{26}$$

The above formula indicates that the curve drops faster at the midpoint $r = R_a$ as the ratio between detector aperture and beam width becomes larger, and this is in line with expectations.

[4]More specifically, (23) can be directly constructed from the Fermi–Dirac distribution, which has these properties of (22). The PDF of Fermi–Dirac distribution is $f = \frac{1}{\exp((E-\mu)/k_{\mathrm{B}}T)+1} = 1 - \frac{1}{1+\exp(-(E-\mu)/k_{\mathrm{B}}T)}$ [20]. Thus, (23) can be obtained by substituting $E, \mu, k_{\mathrm{B}}T$ with $(r/R_a)^{2k}, 1, 1/\alpha$, respectively.

Substituting (26) into (23) gives the result of the point approximation model. Note that (23) is reduced to

$$h_p(r;z) = \exp\left(-\alpha\left[\left(\frac{r}{R_a}\right)^{2k} - 1\right]\right) \tag{27}$$

as $r > R_a$. Hence, based on the (1) and (28), we demonstrate that the parameter k is assigned to be 1 intuitively, and this can be verified based on the numerical results in the next section.

Furthermore, by using the (7) and (23), the PDF of h_p in this case is approximated as

$$f_{h_p}(h_p) = \frac{R_a^2}{2\sigma_s^2}\frac{1}{\alpha}\left[\frac{h_p}{c(1-h_p)}\right]^{\frac{R_a^2}{2\alpha\sigma_s^2}}\frac{1}{h_p(1-h_p)}, \tag{28}$$

where $c = \exp(\alpha)$.

2) Second Reduced Vasylyev Model: As $R_a \gg w_z$, the coefficients λ, R in (16) can be reduced into

$$\lambda = \frac{2\sqrt{2}R_a}{\sqrt{\pi}w_z}\frac{1}{\ln(2)},$$
$$R = R_a\ln(2)^{-1/\lambda}, \tag{29}$$

and a full derivation of (29) is present in Appendix A.

Hence, substituting (29) into (15), the second reduced Vasylyev model is obtained as

$$h_p(r;z) = \exp\left[-\left(\frac{r}{R_a}\right)^{\lambda}\ln(2)\right] = 2^{-\left(\frac{r}{R_a}\right)^{\lambda}}. \tag{30}$$

Correspondingly, by using the (7) and (30), the PDF of h_p in this case is obtained approximately as

$$f_{h_p}(h_p) = \frac{R_a^2}{\ln(2)^{2/\lambda}\sigma_s^2\lambda h_p}\exp\left[-\frac{R_a^2}{2\sigma_s^2}\left(\frac{\ln(1/h_p)}{\ln(2)}\right)^{2/\lambda}\right]$$
$$\times \ln(1/h_p)^{2/\lambda-1}. \tag{31}$$

IV. Numerical Results

In this section, we investigate the effectiveness of the pointing errors models that are present in the previous section. The theoretical results are obtained through MATLAB, and they are also included as a benchmark in all the figures. Moreover, from the perspective of computation efficiency, the number of splits n in the linearized model is set to be 4 if not specified yet. It should be emphasized that the radial distance r_0 in the linearized model is optimized to minimize the NMSE performance, which is defined by $||h-\hat{h}||_2^2/||h||_2^2$ with h and $\hat{h}$ representing the theoretical value and approximate value respectively.

In Fig. 5, we present the theoretical results and approximate results for different models and w_z/R_a. The corresponding NMSE performance is shown in Table I. Note that the normalized optimized radial distance r_0^*/R_a that minimizes the NMSE performance for these three kinds of normalized beam width, i.e., $w_z/R_a = 2, 4, 6$ are $4.05, 12.95, 27.6$ respectively. From this figure, it can be clearly seen that the accuracy of the first reduced Vasylyev model and the intensity uniform model is close

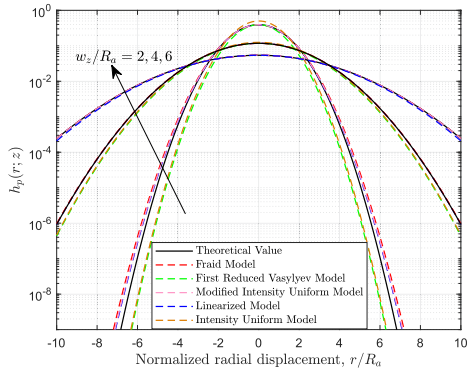

Fig. 5. Theoretical and approximate values of $h_p(r;z)$ for different pointing errors models.

TABLE I
NMSE Performance Between Theoretical Values and Approximate Values for Different Models

Model	$w_z/R_a = 2$	$w_z/R_a = 4$	$w_z/R_a = 6$
Farid Model	1.08×10^{-4}	5.53×10^{-6}	1.13×10^{-6}
First Reduced Vasylyev Model	1.07×10^{-2}	7.17×10^{-4}	1.43×10^{-4}
Modified Intensity Uniform Model	1.94×10^{-5}	8.95×10^{-8}	3.57×10^{-9}
Linearized Model	1.14×10^{-5}	4.85×10^{-8}	1.92×10^{-9}
Intensity Uniform Model	4.62×10^{-2}	2.74×10^{-3}	5.35×10^{-4}

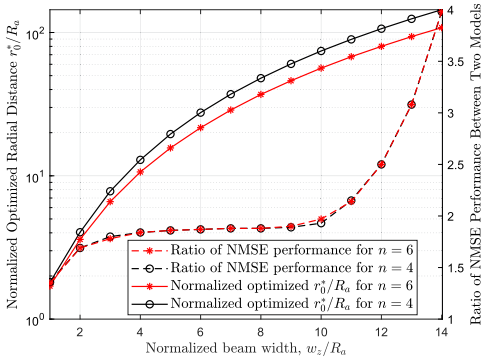

Fig. 6. The normalized optimized radial distance r_0^*/R_a, and the ratio of NMSE performance between modified intensity uniform model and linearized model for different w_z/R_a.

to each other, and they present the poorest approximation accuracy among these models. The accuracy of modified intensity uniform model is comparable with that of linearized model, and the former is more computation-efficient than the latter. Moreover, both of these two models show excellent agreement with the theoretical values even when $w_z/R_a = 2$, where NMSE $\approx 1 \times 10^{-5}$, and are more accurate than the traditional Farid model that is widely used in the FSO systems.

In Fig. 6, we investigate the effects of the normalized beam width w_z/R_a, and the number of splits n on the normalized optimized radial distance r_0^*/R_a and the ratio of NMSE performance. It should be noted that the ratio of

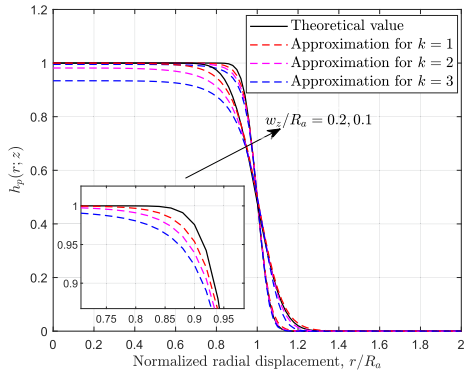

Fig. 7. The approximate values of $h_p(r;z)$ for different k in the point approximation model.

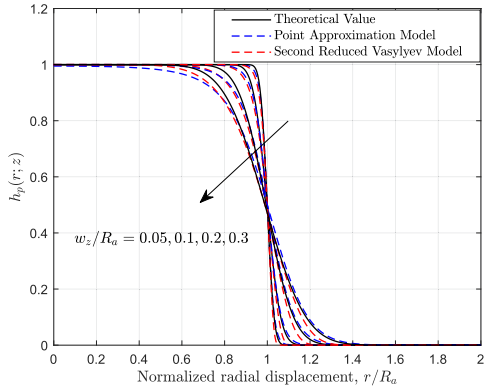

Fig. 8. Theoretical and approximate values of $h_p(r;z)$ for different models.

NMSE performance is derived between the modified intensity uniform model and the linearized model. From this figure, we find that the relation between r_0^*/R_a and w_z/R_a is a quadratic function for these two splits, i.e, the expressions are $r_0^*/R_a = 0.72(w_z/R_a)^2 + 0.08(w_z/R_a) + 1.01$ and $r_0^*/R_a = 0.52(w_z/R_a)^2 + 0.30(w_z/R_a) + 0.93$ for $n = 4, 6$ respectively. Additionally, the R-square is 1 for both of them. As for the ratio of NMSE performance, it can be observed that they are close to each other for two kinds of splits, which indicates that NMSE performance for $n = 4$ and $n = 6$ is nearly equivalent.

Fig. 7 depicts the effects of k in the point approximation model on the approximate accuracy when $w_z/R_a = 0.2$ and $w_z/R_a = 0.1$. Specifically, the corresponding NMSE results for $w_z/R_a = 0.1$ are $5.5 \times 10^{-5}, 1.2 \times 10^{-4}, 3.1 \times 10^{-4}$ for $k = 1, 2, 3$ respectively. As can be seen, the best approximation can be achieved when $k = 1$. As expected, the curve decreases more dramatically at the midpoint $r/R_a = 1$ when w_z/R_a is smaller.

Fig. 8 shows the approximate results of $h_p(r;z)$ for the point approximation model and the second reduced Vasylyev model. In addition, the corresponding NMSE results of these two models are shown in Table II. From this figure, we demonstrate that both of the two models provide an efficient approximation when compared to the theoretical values. However, it can be observed from the NMSE performance in Table II that the proposed point approximation model achieves a higher accuracy than the second reduced Vasylyev model when $w_z/R_a \leq 0.2$.

TABLE II
NMSE PERFORMANCE BETWEEN THEORETICAL VALUES AND APPROXIMATE VALUES FOR DIFFERENT MODELS

w_z/R_a	Point Approximation Model	Second Reduced Vasylyev Model
0.05	6.05×10^{-8}	1.31×10^{-5}
0.1	6.49×10^{-7}	3.04×10^{-5}
0.2	1.11×10^{-5}	4.05×10^{-5}
0.3	8.61×10^{-5}	1.04×10^{-5}

V. CONCLUSION

In this work, we have present several new results for the pointing errors model, and the accuracy of them is investigated in terms of NMSE performance. The linearized model was shown to provide the best approximation among these models, and the normalized optimized radial distance r_0^*/R_a in this model has a quadratic relationship with the normalized beam width w_z/R_a. Also, we demonstrate that the accuracy of the modified intensity uniform model is not only superior to that of the traditional Farid model from the perspective of the numerical results, but also it is expressed in a simpler form. This indicates that our model is preferable in the performance analysis of FSO systems considering the effects of the pointing errors. Furthermore, by analogizing the beam spot with a point when $R_a \gg w_z$, the solution of the pointing errors model is transformed to a smooth function approximation problem, and numerical results show that the proposed pointing approximation model achieves a better approximation than the model developed by Vasylyev when $w_z/R_a \leq 0.2$.

APPENDIX A

According to [19, eqn. (8.451.5)], we have

$$\lim_{x\to\infty} \exp(-x)\, I_v(x) = \frac{1}{\sqrt{2\pi x}} = 0, \tag{32}$$

which leads to

$$\begin{aligned} 1 - \exp\left(-4\frac{R_a^2}{w_z^2}\right) I_0\left(4\frac{R_a^2}{w_z^2}\right) &= 1, \\ \exp\left(-4\frac{R_a^2}{w_z^2}\right) I_1\left(4\frac{R_a^2}{w_z^2}\right) &= \frac{1}{\sqrt{2\pi 4\frac{R_a^2}{w_z^2}}}. \end{aligned} \tag{33}$$

Therefore, combining with the formula $\lim_{R_a/w_z\to\infty} \eta = 1 - \exp(-2R_a^2/w_z^2)$, we can obtain

$$\begin{aligned} \lambda &= \frac{2\sqrt{2}R_a}{\sqrt{\pi}w_z}\frac{1}{\ln(2)} \\ R &= R_a \ln(2)^{-1/\lambda} \end{aligned} \tag{34}$$

after some algebraic manipulations.

REFERENCES

[1] W. Shao et al., "Terabit FSO communication based on a soliton microcomb," *Photon. Res.*, vol. 10, no. 12, pp. 2802–2808, Dec. 2022.

[2] M. Alsabah et al., "6G wireless communications networks: A comprehensive survey," *IEEE Access*, vol. 9, pp. 148191–148243, 2021.

[3] M. Najafi, B. Schmauss, and R. Schober, "Intelligent reflecting surfaces for free space optical communication systems," *IEEE Trans. Commun.*, vol. 69, no. 9, pp. 6134–6151, Sep. 2021.

[4] H. Kaushal and G. Kaddoum, "Optical communication in space: Challenges and mitigation techniques," *IEEE Commun. Surveys Tuts.*, vol. 19, no. 1, pp. 57–96, Firstquarter 2017.

[5] A. Trichili, M. A. Cox, B. S. Ooi, and M.-S. Alouini, "Roadmap to free space optics," *J. Opt. Soc. Amer. B*, vol. 37, no. 11, pp. A184–A201, Nov. 2020.

[6] H. Kaushal, G. Kaddoum, V. Jain, and S. Kar, "Experimental investigation of optimum beam size for FSO uplink," *Opt. Commun.*, vol. 400, pp. 106–114, 2017.

[7] L. C. Andrews and R. L. Phillips, *Laser Beam Propagation Through Random Media*. Bellingham, WA, USA: SPIE Press, 2005.

[8] K. P. Peppas, G. C. Alexandropoulos, E. D. Xenos, and A. Maras, "The Fischer–Snedecor 1-distribution model for turbulence-induced fading in free-space optical systems," *J. Lightw. Technol.*, vol. 38, no. 6, pp. 1286–1295, Mar. 2020.

[9] M. Miao and X. Li, "Parameter estimation of the Lognormal-Rician channel model using saddlepoint approximation," *IEEE Access*, vol. 8, pp. 152924–152931, 2020.

[10] I. S. Ansari, F. Yilmaz, and M.-S. Alouini, "Performance analysis of free-space optical links over málaga ($\mathcal{M}$) turbulence channels with pointing errors," *IEEE Trans. Wireless Commun.*, vol. 15, no. 1, pp. 91–102, Jan. 2016.

[11] R. Esposito, "Power scintillations due to the wandering of the laser beam," *Proc. IEEE*, vol. 55, no. 8, pp. 1533–1534, Aug. 1967.

[12] J. I. Marcum, *Table of Q. Functions*. Santa Monica, CA: RAND Corporation, 1950.

[13] A. A. Farid and S. Hranilovic, "Outage capacity optimization for free-space optical links with pointing errors," *J. Lightw. Technol.*, vol. 25, no. 7, pp. 1702–1710, Jul. 2007.

[14] D. Y. Vasylyev, A. A. Semenov, and W. Vogel, "Toward global quantum communication: Beam wandering preserves nonclassicality," *Phys. Rev. Lett.*, vol. 108, Jun. 2012, Art. no. 220501.

[15] B. E. A. Saleh and M. C. Teich, *Fundamentals of Photonics*, 1st ed. New York, NY, USA: Wiley, 1991. [Online]. Available: https://cds.cern.ch/record/244535

[16] M. M. Agrest, *Theory of Incomplete Cylindrical Functions and Their Applications*. Berlin, Germany: Springer, 1971.

[17] M. Miao and X. Li, "Performance analysis of FSO systems over a Lognormal-Rician turbulence channel with generalized pointing errors," *J. Lightw. Technol.*, vol. 40, no. 13, pp. 4206–4216, Jul. 2022.

[18] K. Singh et al., "Investigations on mode-division multiplexed free-space optical transmission for inter-satellite communication link," *Wireless Netw.*, vol. 28, no. 3, pp. 1003–1016, 2022.

[19] I. S. Gradshteyn and I. M. Ryzhik, *Table of Integrals, Series, and Products*, 7th ed. Amsterdam, The Netherlands: Elsevier/Academic Press, 2007.

[20] S.-C. Kim, A. S. Arun, M. E. Ahsen, R. Vogel, and G. Stolovitzky, "The Fermi–Dirac distribution provides a calibrated probabilistic output for binary classifiers," *Proc. Nat. Acad. Sci.*, vol. 118, no. 34, 2021, Art. no. e2100761118.

[21] F. W. J. Olver, "The asymptotic expansion of Bessel functions of large order," *Phil. Trans. R. Soc. London A*, vol. 247, pp. 328–368, 1954.